Multi-Fidelity Model Management Strategy for Accelerated Antenna Optimization

Slawomir Koziel[1,2][0000-0002-9063-2647], Anna Pietrenko-Dabrowska[2][0000-0003-2319-6782], and Leifur Leifsson[3][0000-0001-5134-870X]

[1] Engineering Optimization & Modeling Center, Department of Engineering, Reykjavík University, Menntavegur 1, 102 Reykjavík, Iceland
koziel@ru.is
[2] Faculty of Electronics Telecommunications and Informatics, Gdansk University of Technology, Narutowicza 11/12, 80-233 Gdansk, Poland
anna.dabrowska@pg.edu.pl
[3] School of Aeronautics and Astronautics, Purdue University, West Lafayette, IN 47907, USA
leifur@purdue.edu

Abstract. Rigorous optimization methods have become standard practice in antenna engineering, gradually replacing traditional interactive design approaches that relied on parametric studies and engineering intuition. Nevertheless, antenna optimization remains computationally expensive due to its reliance on electromagnetic (EM) analysis. To mitigate this, accelerated strategies have been introduced by limiting the occurrences of EM simulations at the algorithmic level or through surrogate modeling. Multi-fidelity approaches offer another avenue, though existing frameworks typically restrict themselves to just two levels (low and high fidelity). In this work, we propose an innovative model management scheme that adaptively adjusts EM model resolution across a continuous fidelity spectrum. Model selection is guided by the optimization's convergence status and design quality indicators. The process begins with the lowest usable resolution, which is progressively refined as the optimization approaches convergence and the objective value improves. This strategy lowers computational costs by exploiting faster, lower-fidelity simulations when far from the optimum, while ensuring reliability by incorporating high-fidelity models near convergence. Extensive numerical experiments involving two microstrip antennas showcase the efficacy of the presented framework, showing speedups of exceeding 70% compared to the baseline approach, with only negligible performance degradation.

Keywords: Antenna engineering, simulation-based optimization, multi-fidelity EM analysis, model management.

1 Introduction

The development of modern antenna systems has become increasingly demanding due to stringent performance requirements driven by emerging applications, e.g., 5G/6G communications, the Internet of Things, wearable devices, and microwave imaging [1]-[4]. These challenges are compounded by the need to address multiple, often

ICCS Camera Ready Version 2026
To cite this paper please use the final published version:
DOI: 10.1007/978-3-032-29909-3_12

conflicting objectives (e.g., impedance bandwidth enhancement and gain improvement [5]) while implementing specific functionalities such as circular polarization or multiple-input multiple-output (MIMO) operation [6]. Consequently, antenna development is a complex, multi-stage process involving geometry evolution, parametric studies [7], and optimization [8]. To ensure reliability, parameter tuning must be conducted using electromagnetic (EM) analysis. However, EM-based design is computationally expensive [9]. While local parameter adjustments may remain tractable [10], more challenging endeavors, for example, global optimization [11] and especially uncertainty quantification [12], often become prohibitively costly when performed solely with EM simulations.

Significant research efforts were devoted to mitigating the challenges of EM-based antenna design. One line of work focuses on more efficient algorithms, particularly gradient-based methods enhanced with adjoint sensitivities [13] or sparse Jacobian updating schemes [14]. Another active direction is surrogate-assisted optimization employing physics-oriented [15] and behavioral models [16]. Data-driven representations, now more prevalent, include traditional regression techniques such as kriging and support vector regression, as well as artificial neural networks [17], [18]. Surrogates are frequently embedded within machine learning (ML) frameworks [19], where they are iteratively refined and exploited to generate candidate solutions throughout the optimization process [20]. Nonetheless, effective behavioral modeling of antennas remains challenging because of the curse of dimensionality and the pronounced frequency response nonlinearity.

Certain optimization scenarios are closely tied to specific applications. For instance, global and multi-objective searches are commonly employed in array pattern synthesis [21] and metasurface design [22]. Nevertheless, the most important procedure in antenna design is local tuning. This reflects the nature of the design workflow, which typically yields reasonable starting points through a mix of geometry evolution, parametric studies, and engineering intuition. Local optimization is predominantly carried out using gradient-based methods. While computationally demanding, these methods can be accelerated with adjoint sensitivities—though their availability in commercial EM solvers remains limited—or through physics-based techniques such as space mapping [23] and response correction [24]. The effectiveness of the latter, however, strongly depends on careful selection of low-fidelity models and correction strategies. Additional speedup can be achieved using sparse sensitivity updating [14], [25], sometimes in combination with response feature technology [26], offering up to 40–50% acceleration, albeit with minor but noticeable degradation in solution quality.

Additional improvements in the practicality of EM-driven local tuning can be achieved by variable-fidelity simulations. However, efficient management of model resolution remains a non-trivial challenge [27], and as a result, most existing frameworks restrict themselves to only two fidelity levels (e.g., [15], [23]). A notable exception is [28], which introduced one of the first practical strategies for continuous fidelity management, where model resolution is adaptively controlled using the convergence indicators of the algorithm, with restarts employed to mitigate premature convergence. While effective in reducing computational cost, the methodology of [28] is conceptually complex and difficult to implement in practice.

ICCS Camera Ready Version 2026
To cite this paper please use the final published version:
DOI: 10.1007/978-3-032-29909-3_12

This study presents an alternative model management strategy, where simulation fidelity is adaptively adjusted based on convergence indicators and the quality of the current design. At the early stages of optimization, the lowest admissible fidelity is employed to minimize cost. The resolution is gradually increased as the algorithm approaches convergence and the objective function attains values consistent with performance requirements. This mechanism provides further acceleration by avoiding high-fidelity evaluations of poor-quality designs. Extensive verification using two wideband antennas and multiple benchmarks demonstrates the remarkable efficiency of the proposed framework, with relative savings exceeding 70% while maintaining reliability. From a practical perspective, an additional strength of the method lies in its simplicity and ease of implementation.

2 Model Management for Multi-Fidelity Antenna Optimization

This section elaborates on the proposed optimization strategy. The emphasis is on variable-resolution model management. The material is structured into five sub-sections. In Section 2.1, we formulate the optimization task. Section 2.2 outlines the baseline gradient-based optimization routine. The concept of variable-fidelity EM models is discussed in Section 2.3. Section 2.4 covers the model management approach. The complete algorithm is summarized in Section 2.5.

2.1 Problem Statement

EM-based optimization is nowadays imperative in antenna design. It requires identification of decision variables (typically, antenna dimensions), merit function, and optional constraints. All practical design tasks are inherently multi-criterial; however, multi-objective optimization [33], [34] is out of the scope of this study. At the presence of several goals, they are normally aggregated [35] or handled as constraints [36]. The notation used in this work is listed in Fig. 1, along with the analytical statement of the optimization problems assuming implicit constraint treatment. Figure 2 discusses representative examples of antenna design tasks.

2.2 Baseline Algorithm: Trust-Region Gradient-Based Routine

The model management methodology suggested in this study can be incorporated into most local optimization routines. Here, we illustrate it for the trust-region (TR) method [37]. Its outline is provided in Fig. 3. An updated design $\boldsymbol{x}^{(i+1)}$ is produced in each iteration by optimizing a linear model $\boldsymbol{L}^{(i)}(\boldsymbol{x})$ of antenna characteristics collectively denoted as $\boldsymbol{R}(\boldsymbol{x})$. For specific outputs, e.g., the reflection coefficient S_{11}, the model would take the form of

$$S_L^{(i)}(\boldsymbol{x}, f) = S_{11}(\boldsymbol{x}^{(i)}, f) + \boldsymbol{G}_S(\boldsymbol{x}^{(i)}, f) \cdot (\boldsymbol{x} - \boldsymbol{x}^{(i)}) \tag{7}$$

In (7), $\boldsymbol{G}_S(\boldsymbol{x}^{(i)},f)$ is the gradient of $|S_{11}|$ at $\boldsymbol{x}^{(i)}$ and frequency f.

The major cost-contributing factor of the algorithm is the sensitivity computation (requiring n extra EM analyses when using finite differences). This cost can be reduced using sparse Jacobian updating strategies, e.g., [25], [30], [38]. Some of these will serve as benchmark in the verification section of this paper.

ICCS Camera Ready Version 2026
To cite this paper please use the final published version:
DOI: 10.1007/978-3-032-29909-3_12

Symbol	Explanation
$\boldsymbol{x} = [x_1 \ldots x_n]^T$	Vector of decision variables, typically geometry parameters of the antenna
$U(\boldsymbol{x})$	Scalar objective function; better designs correspond to lower values of U
$g_k(\boldsymbol{x}) \le 0$, $k = 1, \ldots, n_g$	Optional inequality constraints
$h_k(\boldsymbol{x}) = 0$, $k = 1, \ldots, n_h$	Optional equality constraints

(a)

Design optimization problem: identify the optimum vector of design parameters $\boldsymbol{x}^*$ so that

$$\boldsymbol{x}^* = \arg\min_{\boldsymbol{x}} U(\boldsymbol{x}) \quad (1)$$

Constrained optimization problem with implicit constraint handling (cf. [65])

$$\boldsymbol{x}^* = \arg\min_{\boldsymbol{x}} U_P(\boldsymbol{x}) \quad (2)$$

where U_P is a compound of the function U and the penalty terms of the form

$$U_P(\boldsymbol{x}) = U(\boldsymbol{x}) + \sum_{k=1}^{n_g+n_h} \beta_k c_k(\boldsymbol{x}) \quad (3)$$

Remark 1: $c_k(\boldsymbol{x})$ quantifies constraint violations, whereas β_k are the penalty coefficients.
Remark 2: Penalty function example: assume constraint $S(\boldsymbol{x}) \le -10$ dB (S being the maximum in-band $|S_{11}|$); we have $c(\boldsymbol{x}) = [(S(\boldsymbol{x}) + 10)/10]^2$. The $[\,]^2$ ensures smoothness of U_P at the feasible region boundary.

(b)

Fig. 1. EM-based optimization. Formulation of the problem: (a) terminology, (b) design task.

Design scenario: verbal description	Objective function (1) and constraints	Objective function (3)
Design for the best in-band matching within the frequency band F	$U(\boldsymbol{x}) = S(\boldsymbol{x}) = \max\{f \in F : \lvert S_{11}(\boldsymbol{x},f)\rvert\}$	$U_P(\boldsymbol{x}) = U(\boldsymbol{x})$
Design for maximum average in-band gain (frequency range F); ensure $\lvert S_{11}\rvert \le -10$ dB over F	$U(\boldsymbol{x}) = \bar{G}(\boldsymbol{x}) = \frac{1}{F}\int_F G(\boldsymbol{x},f)df$ Constraint: $\lvert S_{11}(\boldsymbol{x},f)\rvert \le -10$ dB for $f \in F$	$U_P(\boldsymbol{x}) = \bar{G}(\boldsymbol{x}) + \beta_1 c_1(\boldsymbol{x})^2$ where $c_1(\boldsymbol{x}) = \left[\max(S(\boldsymbol{x}) + 10, 0)/10\right]^2$
Design for size reduction of a circularly polarized antenna; ensure that $\lvert S_{11}\rvert \le -10$ dB in frequency range F, and axial ratio does not exceed 3 dB over F	$U(\boldsymbol{x}) = A(\boldsymbol{x})$ Constraints: $AR(\boldsymbol{x},f) \le 3$ dB for $f \in F$ and $\lvert S_{11}(\boldsymbol{x},f)\rvert \le -10$ dB for $f \in F$	$U_P(\boldsymbol{x}) = A(\boldsymbol{x}) + \beta_1 c_1(\boldsymbol{x})^2 + \beta_2 c_2(\boldsymbol{x})^2$ where $c_1(\boldsymbol{x}) = \left[\max(S(\boldsymbol{x}) + 10, 0)/10\right]^2$ $c_2(\boldsymbol{x}) = \left[\max(A_R(\boldsymbol{x}) - 3, 0)/3\right]^2$

Fig. 2. EM-driven antenna optimization. Examples of typical design optimization scenarios.

2.3 Variable-Fidelity EM Models

According to our approach, the search is expedited through multi-fidelity EM analysis. While such techniques are common in high-frequency design (e.g., [15], [23]), they are typically restricted to two levels of resolution (coarse and fine). A flexible means of lowering model resolution is to employ coarse-discretization EM simulations, which, however, reduces accuracy. As a result, the low-fidelity model requires appropriate correction—unless it is used solely for tasks such as parameter-space pre-screening.

The cost–accuracy trade-off is illustrated in Fig. 4 for a broadband antenna, where EM simulation resolution is managed by the LPW (lines-per-wavelength) coefficient in CST Microwave Studio. Using a coarser discretization accelerates the analysis; however, once the mesh density drops below a certain threshold (approximately LPW < 9), the model becomes unreliable due to severely distorted responses. The lowest usable fidelity is therefore defined as $L_{\min}$. The high-fidelity level, $L_{\max}$, is determined through a grid convergence study and corresponds to the LPW value at which further mesh refinement no longer affects the antenna response. In the example considered, this threshold is reached at LPW = 25.

ICCS Camera Ready Version 2026
To cite this paper please use the final published version:
DOI: 10.1007/978-3-032-29909-3_12

In this research, a continuous spectrum of model fidelities within the range $L_{\min} \leq L \leq L_{\max}$ is explored to accelerate antenna optimization. The specific model management strategy is discussed in the next section.

2.4 Model Management

The critical part of the presented algorithm is the appropriate adjustment of EM simulation fidelity during the optimization process. As mentioned earlier, in this study, our model management strategy is integrated with the TR routine elucidated earlier. The model fidelity is adjusted using the coefficient L, and can change between $L_{\min}$ and $L_{\max}$, as elucidated in Section 2.3. Our major concern is to ensure sizable acceleration while retaining the reliability. To achieve that, we observe the following prerequisites:

Problem statement: Solve $\boldsymbol{x}^* = \arg\min\{\boldsymbol{x} \in X : U(\boldsymbol{x})\}$ (cf. (1))

Algorithm operation: Generate a series $\boldsymbol{x}^{(i)}$, $i = 0, 1, \ldots$, of approximations to $\boldsymbol{x}^*$, with $\boldsymbol{x}^{(0)}$ being an initial design. The new vector $\boldsymbol{x}^{(i+1)}$ is obtained by solving

$$\boldsymbol{x}^{(i+1)} = \arg\min_{\boldsymbol{x}: \|\boldsymbol{x}-\boldsymbol{x}^{(i)}\| \leq d^{(i)}} U_L^{(i)}(\boldsymbol{x}) \quad (4)$$

where $U_L^{(i)}$ is analytically identical to U but evaluated using the first-order approximation model $\boldsymbol{L}^{(i)}(\boldsymbol{x})$ of the EM-simulated antenna responses $\boldsymbol{R}(\boldsymbol{x})$, defined at $\boldsymbol{x}^{(i)}$ as

$$\boldsymbol{L}^{(i)}(\boldsymbol{x}) = \boldsymbol{R}(\boldsymbol{x}^{(i)}) + \boldsymbol{J}_R(\boldsymbol{x}^{(i)}) \cdot (\boldsymbol{x} - \boldsymbol{x}^{(i)}) \quad (5)$$

The Jacobian matrix, JR, is estimated using finite differences.

Gain ratio r: EM-evaluated versus linear-model predicted objective function improvement

$$r = \frac{U(\boldsymbol{x}^{(i+1)}, F) - U(\boldsymbol{x}^{(i)}, F)}{U_L(\boldsymbol{x}^{(i+1)}, \boldsymbol{L}^{(i)}(\boldsymbol{x}^{(i+1)}), F) - U_L(\boldsymbol{x}^{(i)}, \boldsymbol{L}^{(i)}(\boldsymbol{x}^{(i)}), F)} \quad (6)$$

Trust region size $d^{(i)} > 0$: Adaptively adjusted based on r; $d^{(i+1)} = d^{(i)} m_{incr}$ if $r > r_{incr}$, and $d^{(i+1)} = d^{(i)}/m_{decr}$ if $r < r_{decr}$; standard control parameter values are $r_{incr} = 0.75$, $r_{decr} = 0.25$, $m_{incr} = 1.5$, $m_{decr} = 2$ [67].

Acceptance of the new iteration point: $\boldsymbol{x}^{(i+1)}$ is accepted only if $r > 0$ (i.e., EM-evaluated objective function has been improved); otherwise, the iteration is repeated with reduced TR size;

Algorithm termination: Convergence in argument ($\|\boldsymbol{x}^{(i+1)} - \boldsymbol{x}^{(i)}\| < \varepsilon_{TR}$) or sufficient reduction of the TR size ($d^{(i)} \leq \varepsilon_{TR}$); the termination threshold is set to $\varepsilon_{TR} = 10^{-3}$

Fig. 3. Baseline TR gradient-based routine: the outline.

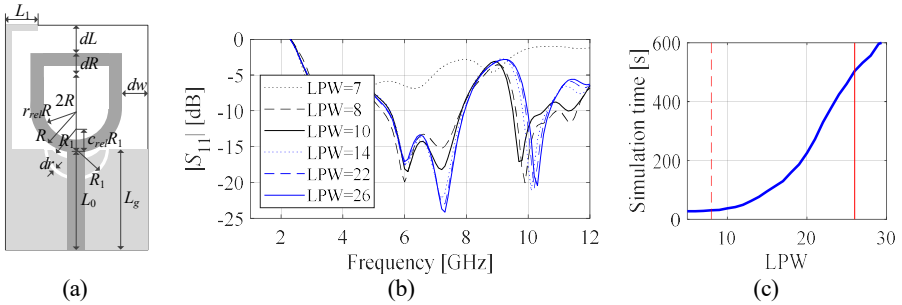

(a) (b) (c)

Fig. 4. Multi-fidelity EM analysis for a broadband antenna: (a) antenna topology, (b) $|S_{11}|$ for various mesh densities controlled using the LPW parameter, (c) LPW vs. simulation time. The LPW of the high-fidelity and the lowest usable low-fidelity models are represented by solid and dashed lines.

ICCS Camera Ready Version 2026
To cite this paper please use the final published version:
DOI: 10.1007/978-3-032-29909-3_12

- To expedite the process, it should start from the lowest allowed fidelity.
- When approaching convergence, the high-fidelity model must be applied for quality.
- The model fidelity adjustment should be based on convergence indicators, such as the iteration point distance $\|\boldsymbol{x}^{(i+1)} - \boldsymbol{x}^{(i)}\|$.
- The resolution changes should also be a function of design quality assessed using the merit function value $U(\boldsymbol{x}^{(i)})$ at the current iteration. In particular, poor designs should be evaluated at lower fidelity levels to reduce the computational effort.
- For stability, the fidelity adjustments should be monotonic regarding the mentioned factors.

We denote as $\varepsilon = \varepsilon_{TR}$ the algorithm's termination threshold; the search is stopped if $\|\boldsymbol{x}^{(i+1)} - \boldsymbol{x}^{(i)}\| < \varepsilon_{TR}$, cf. Fig. 3. Here, we set $\varepsilon = 10^{-3}$. Let $Q_c^{(i)}$ and $Q_q^{(i)}$ be the convergence and the quality factors:

$$Q_c^{(i)} = \log\left(\frac{\|\boldsymbol{x}^{(i+1)} - \boldsymbol{x}^{(i)}\|}{\varepsilon}\right) \tag{8}$$

$$Q_q^{(i)} = U\left(\boldsymbol{x}^{(i)}\right) \tag{9}$$

We also define the lower/upper bounds $Q_{c.\min}$ and $Q_{c.\max}$ for Q_c that determine whether the optimization process is close to ($Q_c^{(i)} < Q_{c.\min}$) or away from convergence ($Q_c^{(i)} > Q_{c.\max}$). We use $Q_{c.\min} = 1$ (one decade from convergence on a logarithmic scale) and $Q_{c.\max} = 3$. The EM simulation fidelity starts increasing when $Q_c^{(i)} < Q_{c.\max}$ and reaches the maximum value regarding this criterion when $Q_c^{(i)} > Q_{c.\min}$.

For design quality, we set $Q_{q.\min}$ and $Q_{q.\max}$ to be the lower/upper bounds on Q_q that determine whether the design quality is satisfactory ($Q_q^{(i)} < Q_{q.\min}$) or is poor ($Q_q^{(i)} > Q_{q.\max}$). As the design tasks considered in Sectio 3 are oriented towards matching improvement with the objective function defined as in Fig. 2, we set $Q_{q.\min} = -10$ dB and $Q_{q.\max} = -6$ dB. The EM analysis fidelity starts increasing when $Q_q^{(i)} < Q_{q.\max}$ and reaches the maximum value regarding this criterion when $Q_q^{(i)} > Q_{q.\min}$.

The final component is a transition function T, defined as follows:

$$T(q, q_{\min}, q_{\max}) = \begin{cases} 1 \text{ if } q < q_{\min} \\ (q_{\max} - q)/(q_{\max} - q_{\min}) \text{ if } q_{\min} \le q \le q_{\max} \\ 0 \text{ if } q > q_{\max} \end{cases} \tag{10}$$

The model resolution at the ith iteration is adjusted based on the following relationship:

$$L^{(i+1)} = \max\left\{L^{(i)}, L_{\min} + \left(L_{\max} - L_{\min}\right) T(Q_c^{(i)}, Q_{c.\min}, Q_{c.\max}) T(Q_q^{(i)}, Q_{q.\min}, Q_{q.\max})\right\} \tag{11}$$

where $L^{(0)} = L_{\min}$. Observe that $L^{(i)}$ depends on both the convergence status and design quality. If a satisfactory design is attainable (i.e., $Q_q(\boldsymbol{x}) < Q_{q.\min}$ for certain $\boldsymbol{x}$), then the model fidelity increases to $L_{\max}$ when close to convergence (i.e., when $Q_c(\boldsymbol{x}) < Q_{c.\min}$), which ensures the application of the high-resolution EM model at the late search steps. Otherwise, a high-fidelity model will never be employed.

Note that the proposed model management strategy is significantly simpler than the scheme suggested in [28]. In particular, the latter necessitates re-starting the algorithm if the high-fidelity model was not applied until convergence. A graphical representation of model fidelity adaptation has been shown in Fig. 5, showcasing the convergence and design quality indicators and their transformation using the transition function T.

ICCS Camera Ready Version 2026
To cite this paper please use the final published version:
DOI: 10.1007/978-3-032-29909-3_12

Additional speedup is achieved by carrying out the finite differentiation process (employed to compute the antenna Jacobian matrix) at the lower fidelity level L_{FD}, which is adjusted as

$$L_{FD} = \max\left\{L_{\min}, \lambda L^{(i)}\right\} \tag{12}$$

The control parameter $\lambda = 2/3$ as suggested in [28]. This is justified by the fact that models at different fidelity levels are governed by the same underlying physics, ensuring strong correlation despite potentially large absolute response discrepancies.

2.5 Complete Procedure

Figure 6 presents the block diagram of the complete algorithm, which integrates the proposed model management scheme into the TR algorithm covered in Section 2.2. Table 1 enlists the control parameters. Note that their setup is straightforward. In all verification experiments discussed in Section 3, the default values (last column of Table 1) are applied, with one exception: $Q_{q.\min}$. This parameter is adjusted for each design task based on prior knowledge of the attainable objective function level, which may be lower than –10 dB.

3 Results

The optimization algorithm introduced in Section 2 is showcased here based on two planar antennas, and juxtaposed against a range of state-of-the-art procedures, including the baseline TR routine, two expedited versions incorporating sparse sensitivity updating strategies [29], [30], and a multi-fidelity framework [28]. The performance figures are cost efficiency and dependability, measured using the achieved objective function value at the final design.

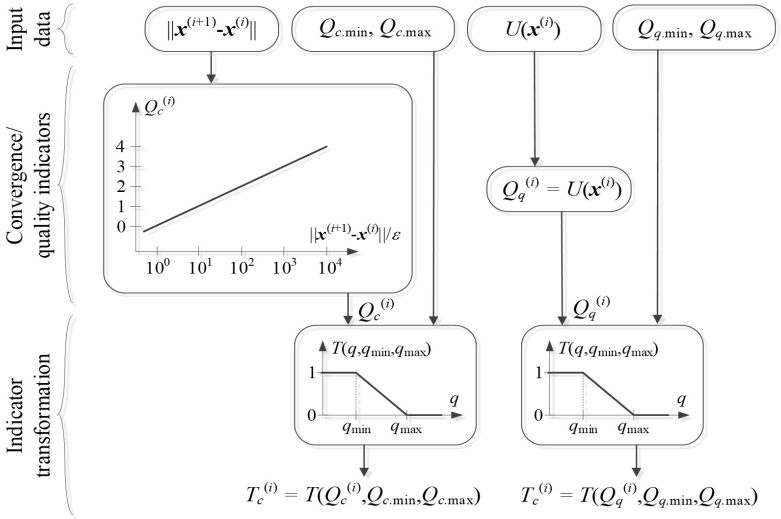

Fig. 5. Convergence and quality indicator computation (8), (9), and their transformation using the transition function T of (10).

ICCS Camera Ready Version 2026
To cite this paper please use the final published version:
DOI: 10.1007/978-3-032-29909-3_12

Table 1. Control parameters

Parameter	Description	Default value
ε_{TR}	Termination threshold (cf. Section 2.2)	10^{-3}
λ	Multiplier for setting model fidelity level L_{FD} for finite differentiation, cf. (12)	2/3
$Q_{c.min}$	Lower bound for the convergence indicator Q_c to determine whether the optimization process is close to convergence (cf. Section 2.4)	1
$Q_{c.max}$	Upper bound for the convergence indicator Q_c to determine whether the optimization process is close to convergence (cf. Section 2.4)	3
$Q_{q.min}$	Lower bound for the quality indicator Q_q to determine whether the current design satisfies the design specifications (cf. Section 2.4)	–10 dB
$Q_{q.max}$	Upper bound for the quality indicator Q_q to determine whether the current design is close to satisfying the design specifications (cf. Section 2.4)	–6 dB

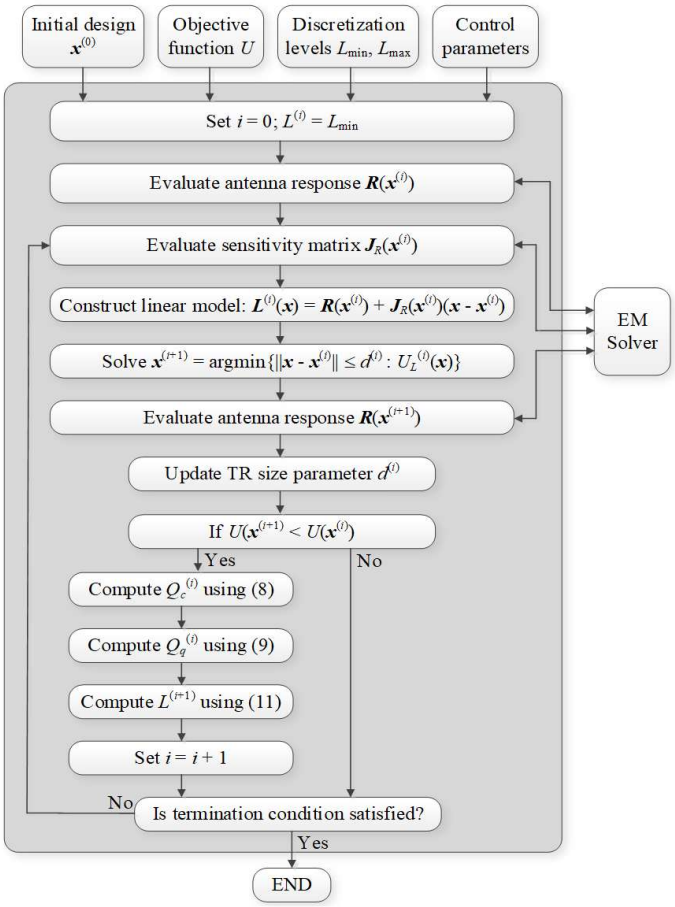

Fig. 6. Block diagram of the presented algorithm with convergence- and design-quality-based model management.

ICCS Camera Ready Version 2026
To cite this paper please use the final published version:
DOI: 10.1007/978-3-032-29909-3_12

3.1 Test Cases and Algorithm Setup. Benchmark Algorithms

Figure 7 shows the verification antennas. The EM models are prepared in CST. Both devices are designed to reduce the maximum in-band $|S_{11}|$ level in the ultra-wideband spanned between 3.1 GHz and 10.6 GHz. The objective function takes the form of $U(\boldsymbol{x}) = \max\{3.1\text{ GHz} \le f \le 10.6\text{ GHz} : |S_{11}(\boldsymbol{x},f)|\}$. The multi-fidelity model setup is provided in Fig. 8. The evaluation time ratio between the highest- and lowest-fidelity models ($L_{\max}$ and $L_{\min}$) ranges from six for Antenna II to ten for Antenna I, which indicates a potentially significant acceleration that may be obtained by incorporating the proposed approach.

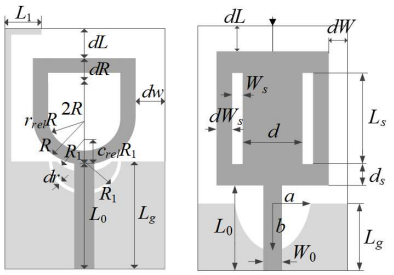

(a) (b)

Antenna	Substrate	Design variables [mm]
I [31]	RF-35 (ε_r = 3.5, h = 0.762 mm)	$\boldsymbol{x}$ = [L_0 dR R r_{rel} dL dw Lg L_1 R_1 dr c_{rel}]^T
II [32]	FR4 (ε_r = 4.3, h = 1.55 mm)	$\boldsymbol{x}$ = [L_g L_0 L_s W_s d dL d_s dW_s dW a b]^T

(c)

Fig. 7. Test antennas (ground planes are distinguished using the light gray color): (a) geometry of Antenna I, (b) geometry of Antenna II, (c) substrate parameters and design variables.

Antenna I: Multi-fidelity EM model setup		
Lowest-fidelity model	$L_{\min}$	11
	Simulation time [s]	41
High-fidelity model	$L_{\max}$	24
	Simulation time [s]	424

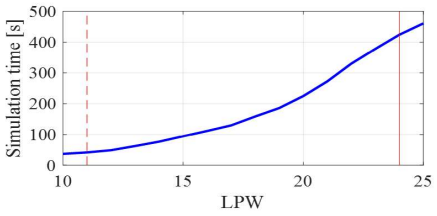

(a)

Antenna II: Multi-fidelity EM model setup		
Lowest-fidelity model	$L_{\min}$	10
	Simulation time [s]	46
High-fidelity model	$L_{\max}$	20
	Simulation time [s]	256

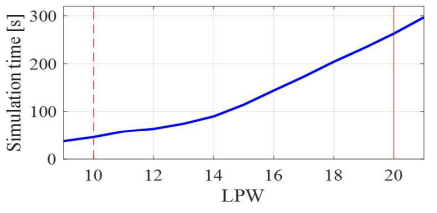

(b)

Fig. 8. Multi-fidelity model setup: (a) Antenna I, (b) Antenna II. The right panel shows the dependence of the simulation time on LPW. The fidelity levels $L_{\min}$ and $L_{\max}$ are marked by dashed and solid lines, respectively.

ICCS Camera Ready Version 2026
To cite this paper please use the final published version:
DOI: 10.1007/978-3-032-29909-3_12

To ensure a meaningful evaluation, the antennas were optimized several times using randomly selected starting points, thereby reducing bias from the starting conditions. Since the test cases are inherently multimodal and all considered algorithms are gradient-based, different initial points may converge to different local optima. Conducting multiple optimization runs enables the assessment of average performance regarding both cost efficiency and dependability.

The proposed algorithm is benchmarked against four reference techniques:

- Algorithm 1: Baseline TR algorithm relying solely on high-fidelity EM simulations.
- Algorithm 2: Accelerated TR algorithm [29], also based exclusively on high-fidelity EM simulations. Its primary speedup mechanism suppresses selected finite-difference (FD)-based Jacobian updating depending on the amplitude of design changes compared to the current TR search region diameter.
- Algorithm 3: Accelerated TR algorithm [30], again using only high-fidelity EM simulations. Here, FD-based sensitivity updates are replaced by the rank-one Broyden formula along the directions that are well-aligned with the design relocation at the most recent iteration.
- Algorithm 4: Multi-fidelity TR algorithm [28], employing a continuous spectrum of EM model fidelities with model management guided by convergence indicators.

The performance metrics of interest are:

- Cost efficiency, measured as the number of equivalent high-fidelity EM simulations.
- Quality, quantified as the mean merit function value for ten independent runs.
- Result consistency, expressed by the standard deviation of the merit function.

Given the test problem multimodality, a nonzero standard deviation is expected even for the baseline method. Thus, any potential consistency loss is assessed relative to Algorithm 1 rather than against a zero standard deviation.

3.2 Results and Discussion

The results, generated from ten independent runs of each method, initialized with random starting points, can be found in Tables 2 and 3. The data include computational cost, savings relative to the baseline (Algorithm 1), average objective function values, and quality degradation compared to Algorithm 1. Figures 9 and 10 illustrate antenna characteristics and the fidelity progression of the proposed method for a representative run. The following conclusions can be formulated:

- *Significant acceleration*: The proposed framework achieves speedups of 70% or more over the baseline, i.e., three to four times faster than Algorithm 1.
- *Correlation with model fidelity ratio*: The achieved savings scale with the runtime ratio between the highest- and lowest-fidelity models ($L_{\max}/L_{\min}$). This ratio is 10.3 for Antenna I and 5.8 for Antenna II, leading to respective cost reductions of 76% and 70%.

ICCS Camera Ready Version 2026
To cite this paper please use the final published version:
DOI: 10.1007/978-3-032-29909-3_12

- *Superiority over expedited TR methods*: For Antenna II, Algorithms 2 and 3 yield average savings of 40% and 31%, respectively, versus 76% and 70% for the proposed approach.
- *Advantage over multi-fidelity TR*: Relative to Algorithm 4 [28], our method delivers an additional 22% savings for Antenna II. For Antenna I, costs are comparable, yet our procedure is simpler to implement and more reliable.

Table 2. Antenna I: results and benchmarking

Algorithm	Performance figure				
	Cost[1]	Cost savings[2]	max|S_{11}|[3]	Δ max|S_{11}|[4]	Std max|S_{11}|[5]
Conventional TR search	111.2	–	–14.9	–	0.6
Accelerated TR search [30]	58.3	48%	–13.7	1.2	1.3
Accelerated TR search [29]	75.9	32%	–14.3	0.6	1.0
Multi-fidelity [28]	25.8	77%	–13.8	1.1	1.0
Multi-fidelity (this work)	27.2	76%	–14.6	0.3	0.7

[1] Number of equivalent high-fidelity EM simulations averaged over 10 algorithm runs.
[2] Relative computational savings in percent w.r.t. the reference algorithm.
[3] Objective function value (maximum in-band reflection in dB), averaged over 10 algorithm runs.
[4] Degradation of max|S_{11}| w.r.t. the reference algorithm in dB, averaged over 10 algorithm runs.
[5] Standard deviation of max|S_{11}| in dB across the set of 10 algorithm runs.

Table 3. Antenna II: results and benchmarking

Algorithm	Performance figure				
	Cost[1]	Cost savings[2]	max|S_{11}|[3]	Δ max|S_{11}|[4]	Std max|S_{11}|[5]
Conventional TR search	111.0	–	–13.9	–	1.0
Accelerated TR search [30]	73.1	34%	–12.8	1.1	1.3
Accelerated TR search [29]	80.0	28%	–11.9	1.9	2.0
Multi-fidelity [28]	42.3	62%	–11.3	2.6	1.0
Multi-fidelity (this work)	33.1	70%	–11.6	2.3	1.0

[1] Number of equivalent high-fidelity EM simulations averaged over 10 algorithm runs.
[2] Relative computational savings in percent w.r.t. the reference algorithm.
[3] Objective function value (maximum in-band reflection in dB), averaged over 10 algorithm runs.
[4] Degradation of max|S_{11}| w.r.t. the reference algorithm in dB, averaged over 10 algorithm runs.
[5] Standard deviation of max|S_{11}| in dB across the set of 10 algorithm runs.

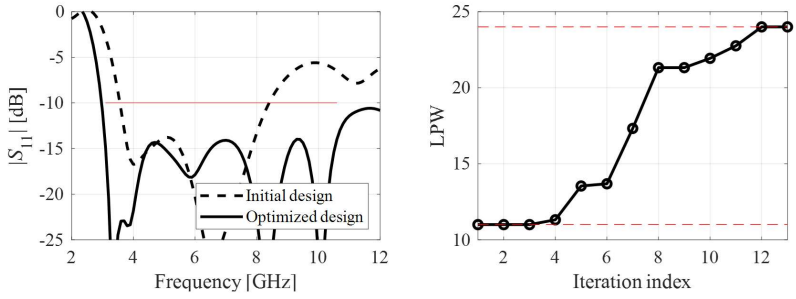

(a) (b)

Fig. 9. Antenna I: (a) $|S_{11}|$ for the chosen run of the presented procedure: (- - -) starting point, (—) final design; (b) history of the model resolution; horizontal lines mark the lowest (L_{min}) and the highest (L_{max}) fidelity levels.

ICCS Camera Ready Version 2026
To cite this paper please use the final published version:
DOI: 10.1007/978-3-032-29909-3_12

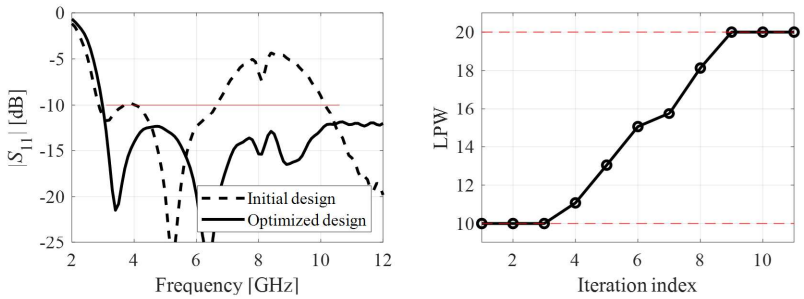

(a) (b)

Fig. 10. Antenna II: (a) $|S_{11}|$ for the chosen run of the presented procedure: (- - -) starting point, (—) final design; (b) history of the model resolution; horizontal lines mark the lowest ($L_{\min}$) and the highest ($L_{\max}$) fidelity levels.

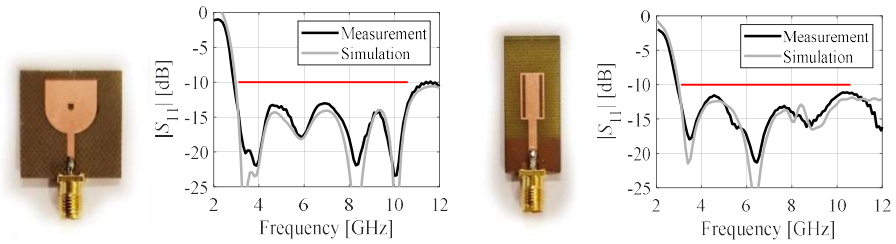

(a) (b)

Fig. 11. Experimental validation of the test antennas at the optimized designs shown in Figs. 3 and 4: (a) Antenna I, (b) Antenna II. Target bandwidth marked using a horizontal line.

- *Minimal quality loss*: For Antenna I, degradation is negligible (a fraction of a dB in the minimax objective). For Antenna II, the loss is the highest (about 2 dB), yet it is comparable to other benchmarks and lower than Algorithm 4, which uses multi-fidelity EM models, though its fidelity adjustment scheme is considerably more complex.
- *Consistency*: The standard deviation of the merit function is on par with the baseline, confirming robustness across multiple runs.

In summary, the presented multi-fidelity management scheme yields substantial computational savings with only minor quality trade-offs. Its simplicity and reliability make it a practical alternative to existing schemes such as [28]. Future work will focus on further cost reductions, particularly through sparse sensitivity update mechanisms as in [29] and [30].

3.3 Experimental Validation

Further validation of the proposed procedure was performed through prototyping and experimental testing of the optimized designs of Antennas I and II, specifically the rep-

ICCS Camera Ready Version 2026
To cite this paper please use the final published version:
DOI: 10.1007/978-3-032-29909-3_12

resentative cases shown in Figs. 9 and 10. As depicted in Fig. 11, the measured responses agree well with the EM-evaluated results across the considered frequency band. Only minor deviations are observed, which can be attributed to fabrication tolerances and assembly imperfections. It is worth noting that the accuracy of the EM simulations was enhanced by explicitly incorporating the SMA connectors into the computational models of both antennas.

4 Conclusion

This paper introduces an innovative procedure for accelerated gradient-based parameter tuning of antennas. The proposed framework leverages a continuous spectrum of variable-fidelity EM antenna representations together with a fidelity management strategy that dynamically adjusts simulation accuracy during the optimization process. Fidelity selection is governed by algorithm convergence status and design quality: the search begins with the lowest admissible resolution and progressively transitions to high-fidelity analysis near convergence. This strategy yields substantial savings, exceeding 70% relative to the baseline algorithm, while preserving reliability. The efficacy of the approach was validated on two broadband antennas and compared to several state-of-the-art methods, both traditional and expedited. Results also indicate a notable speedup of over 20% compared with the most recent multi-fidelity management technique. The method offers several additional benefits, including ease of implementation and straightforward handling. Future research will focus on integrating further acceleration mechanisms and extending the framework to other classes of antennas (e.g., multi-band antennas) and microwave structures (such as couplers of power dividers).

Acknowledgement

The authors would like to thank Dassault Systemes, France, for making CST Microwave Studio available. This work is partially supported by the Icelandic Research Fund Grant 239858 and by the National Science Centre of Poland Grant 2024/55/B/ST7/01413.

References

1. Kim, T.-H., Elhefnawy, M., Kim, K.-H., Lee, W.-S. Dual circularly polarized bow-tie-shaped stacked Yagi-Uda antenna arrays for internet of things applications. *IEEE Access*, **13**, 34070–34080 (2025)
2. Cheng, S.-H., Chen, S.-C., Huang, W.-Y. Low-profile MIMO trapezoidal patch antenna for 5G wideband mobile antenna application. *IEEE Ant. Wireless Propag. Lett.*, **24**, 696–700 (2025)
3. Cheng, J., *et al.*, A compact low-profile vehicular 5G MIMO antenna system. *IEEE Ant. Wireless Propag. Lett.*, **24**, 2422–2426 (2025)
4. Su, W., Prasannakumar, P.V., Li, Y., Ye, G., Zhu, J., Wearable antennas for virtual reality cross-body links. *IEEE Open J. Ant. Propag.*, **4**, 207–215 (2023)

ICCS Camera Ready Version 2026
To cite this paper please use the final published version:
DOI: 10.1007/978-3-032-29909-3_12

5. Esmail, B.A.F., Isleifson, D., Koziel, S. Millimeter-wave Yagi MIMO antenna with high isolation and beam-tilting capability using optimized metamaterials. *IEEE Access*, **13**, 107710–107719 (2025)
6. Tuan Le, T., Kim, Y.-D., Yun, T.-Y. Broadband dual-sense circular-polarization reconfigurable metasurface antenna for wearable applications. *IEEE Access*, **13**, 130138–130146 (2025)
7. Huang, H., Ye, J., Xue, C., Li, T. Circular polarization selective metasurface for folded reflectarray antenna at Ka band. *IEEE Ant. Wireless Propag. Lett.*, **24**, 1278–1282 (2025)
8. Lei, S., Yang, Y., Hu, H., Zhao, Z., Chen, B., Qiu, X. Power gain optimization method for wide-beam array antenna via convex optimization. *IEEE Trans. Ant. Prop.*, **67**, 1620–1629 (2019)
9. Koziel, S., Pietrenko-Dabrowska, A., Globalized parameter tuning of microwave passives by dimensionality-reduced surrogates and multi-fidelity simulations. *Sc. Rep.*, **15**, paper no. 21776, (2025)
10. Lu, W., *et al.*, Design of microwave ablation antenna for flexible omnidirectional/directional ablation zone control. *IEEE Ant. Wireless Prop. Lett.*, **24**, 18–22 (2025)
11. Gao, T.-Y., Jiao, Y.-C., Zhang, Y.-X., Zhang, L. A hybrid self-adaptive differential evolution algorithm with simplified bayesian local optimizer for efficient design of antennas. *IEEE Trans. Ant. Prop.*, **73**, 391–404 (2025)
12. Koziel, S., Haq, T., Computationally-efficient statistical design and yield optimization of resonator-based notch filters by feature-based surrogates. *Sc. Rep.*, **13**, paper no. 14823, (2023)
13. Wang, L.-L., Yang, X.-S., Adjoint sensitivity analysis based on well-conditioned asymptotic waveform evaluation for broadband antenna topology optimization acceleration. *IEEE Trans. Ant. Propag.*, **73**, 87–95 (2025)
14. Pietrenko-Dabrowska, A., Koziel, S., Computationally-efficient design optimization of antennas by accelerated gradient search with sensitivity and design change monitoring. *IET Microwaves Ant. Prop.*, **14**, 165–170 (2020)
15. Zhang, J., Yan, X., Luo, H., Guo, Y. An efficient transistor-model-assisted layout synthesis approach using improved implicit space mapping for high-performance MMIC PAs. *IEEE Trans. Circuits Syst. II: Express Briefs*., **71**, 2639–2643 (2024)
16. Chen, W., Wu, Q., Wei, J., Yu, C., Wang, H., Hong, W. Knowledge-guided and machine-learning-assisted synthesis for series-fed microstrip antenna arrays using base element modeling. *IEEE Trans. Ant. Propag.*, **72**, 1497–1509 (2024)
17. Liu, Y., Chen, P., Tian, J., Xiao, J., Noghanian, S., Ye, Q. Hybrid ANN-GA optimization method for minimizing the coupling in MIMO antennas. *AEU – Int. J. Electronics Comm.*, **175**, paper no. 155068 (2024)
18. Tan, J., Shao, Y., Zhang, J., Zhang, J. Efficient antenna modeling and optimization using multifidelity stacked neural network. *IEEE Trans. Antennas Propag.*, **72**, 4658–4663 (2024)
19. Yahya, M.S., Soeung, S., Rahim, S.K.A., Musa, U., Ba Hashwan, S.S., Haque, M.A. Machine learning-optimized compact frequency reconfigurable antenna with RSSI enhancement for long-range applications. *IEEE Access*, **12**, 10970–10987 (2024)
20. He, Y., Huang, J., Li, W., Zhang, L., Wong, S.W., Chen, Z.N. Hybrid method of artificial neural network and simulated annealing algorithm for optimizing wideband patch antennas. *IEEE Trans. Antennas Propag.*, **72**, 944–949 (2024)

ICCS Camera Ready Version 2026
To cite this paper please use the final published version:
DOI: 10.1007/978-3-032-29909-3_12

21. Zhou, Z., Wei, Z., Ren, J., Yin, Y., Pedersen, G.F., Shen, M. Two-order deep learning for generalized synthesis of radiation patterns for antenna arrays. *IEEE Trans. Art. Intel.*, **4**, 1359–1368 (2023)
22. Abdullah, M., Koziel, S., Supervised-learning-based development of multi-bit RCS-reduced coding metasurfaces. *IEEE Trans. Microwave Theory Techn.*, **70**, 264–274 (2021)
23. Gu, P., Cao, Z., He, Z., Ding, D. Design of ultrawideband RCS reduction metasurface using space mapping and phase cancellation. *IEEE Ant. Wireless Prop. Lett.*, **22**, 1386–1390 (2023)
24. Koziel, S., Leifsson, L. Simulation-driven design by knowledge-based response correction techniques, Springer, New York (2016)
25. Koziel, S., Pietrenko-Dabrowska, A., Variable-fidelity simulation models and sparse gradient updates for cost-efficient optimization of compact antenna input characteristics. *Sensors*., **19**, no. 8 (2019)
26. Pietrenko-Dabrowska, A., Koziel, S., Response feature technology for high-frequency electronics. Optimization, modeling, and design automation, Springer, New York, (2023)
27. Ogurtsov, S., Koziel, S., Model management for cost-efficient surrogate-based optimization of antennas using variable-fidelity electromagnetic simulations. *IET Microwaves Ant. Prop.*, **6**, 1643–1650 (2012)
28. Pietrenko-Dabrowska, A., Koziel, S., Accelerated gradient-based optimization of antenna structures using multi-fidelity simulation models. *IEEE Trans. Ant. Propag.*, **69**, 8778–8789 (2021)
29. Koziel, S., Pietrenko-Dabrowska, A., Expedited optimization of antenna input characteristics with adaptive Broyden updates, *Eng. Comp.*, **37**, 3 (2019)
30. Koziel, S., Pietrenko-Dabrowska, A., Reduced-cost electromagnetic-driven optimization of antenna structures by means of trust-region gradient-search with sparse Jacobian updates, *IET Microwaves Ant. Prop.*, **13**, 10, 1646–1652 (2019)
31. Alsath, M.G.N., Kanagasabai, M., Compact UWB monopole antenna for automotive communications, *IEEE Trans. Ant. Prop.*, **63**, 9, 4204–4208 (2015)
32. Haq, M.A., Koziel, S., Simulation-based optimization for rigorous assessment of ground plane modifications in compact UWB antenna design, *Int. J. RF Microwave CAE*, **28**, 4, paper no. e21204 (2018)
33. Zhang, C., Fu, X., Chen, X., Peng, S., Min, X., Synthesis of uniformly excited sparse rectangular planar array for sidelobe suppression using multi-objective optimization algorithm, *J. Eng.*, **2019**, 19, 6278–6281 (2019)
34. Koziel, S., Pietrenko-Dabrowska, A., Fast multi-objective optimization of antenna structures by means of data-driven surrogates and dimensionality reduction, *IEEE Access*, **8**, 183300–183311 (2020)
35. Marler, R.T., Arora, J.S., The weighted sum method for multi-objective optimization: new insights, *Structural Multidisc. Opt.*, **41**, 853–862 (2010)
36. Ullah, U., Koziel., S., Mabrouk, I.B., Rapid re-design and bandwidth/size trade-offs for compact wideband circular polarization antennas using inverse surrogates and fast EM-based parameter tuning, *IEEE Trans. Ant. Prop.*, **68**, 1, 81–89 (2019)
37. Conn, A.R., Gould, N.I.M., Toint, P.L., *Trust Region Methods*, MPS-SIAM Series on Optimization (2000)
38. Pietrenko-Dabrowska, A., Koziel, S., Numerically efficient algorithm for compact microwave device optimization with flexible sensitivity updating scheme, *Int. J. RF & Microwave CAE*, **29**, 7, paper no. e21714 (2019)

ICCS Camera Ready Version 2026
To cite this paper please use the final published version:
DOI: 10.1007/978-3-032-29909-3_12